

**Republic of Iraq Ministry of Higher Education and Scientific
Research**



**University of Diyala
College of Science
Department of Physics**



Synthesis and Characterization of CZTS and CZTSe Quaternary Compounds for Solar Cells Applications

A Dissertation

Submitted to the Council of College of Science University of Diyala in
Partial Fulfillment of the Requirements for the Degree of Doctor of
Philosophy in Physics

By

Ali Talib Abbood

B.Sc. in Physics, 2003

M.Sc. in Physics, 2016

Supervised by

Prof. Dr.

Nabeel Ali Bakr

2023 A.D.

Chief Researchers. Dr.

Falah Ibrahim Mustafa

1444 A.H.

بِسْمِ اللَّهِ الرَّحْمَنِ الرَّحِيمِ

﴿هُوَ الَّذِي بَعَثَ فِي الْأُمِّيِّينَ رَسُولًا مِنْهُمْ يَتْلُو عَلَيْهِمْ آيَاتِهِ وَيُزَكِّيهِمْ وَيُعَلِّمُهُمُ الْكِتَابَ وَالْحِكْمَةَ وَإِنْ كَانُوا مِنْ قَبْلُ لَفِي ضَلَالٍ مُبِينٍ﴾

(سورة الجمعة: الآية 2)

DEDICATION

To the one who encouraged me to persevere all my life, to the most prominent man in my life

(dear father)

To the giving heart

(My beloved mother)

To those who made an effort to help me and were the best support

(My family and my friends)

To everyone who contributed even a letter to my academic life

To all of them: I dedicate this work, which I ask God Almighty to accept sincerely

Ali

ACKNOWLEDGEMENTS

I would like to deliver my sincerest praise and thanks to **Allah**. I would like to thank my supervisor ***Prof. Dr. Nabeel Ali Bakr*** and ***Dr. Falah I. Mustafa*** for their support, inspiration, and valuable advice for this dissertation. I would like to greatly thank special thanks to the Dean of the College of Science, ***Prof. Dr. Tahseen H. Mubarak*** and the head of the Physics Department, ***Dr. Ammar Ayesh***, and all the staff of the Department of Physics for their assistance.

I would like to express my profound gratitude to ***prof. Dr. Ziad Tariq Khodair*** for his kind cooperation and constant support and ***Prof. Dr. Sabah Anwer Salman***, for his constant encouragement throughout my studies.

Special thanks to my friends who stand along with me ***Dr. Muhammad Hameed AL-Timimi*** and ***Dr. Obaida Amer***.

Finally, I would like to thank ***Dr. Susan Abdul Raheem Hasan*** for helping and encouraging me in this work.

ABSTRACT

$\text{Cu}_2\text{ZnSnS}_4$ (CZTS) and $\text{Cu}_2\text{ZnSnSe}_4$ (CZTSe), are copper zinc tin sulfide, and selenide materials. They are developing as promising new long-term light absorption materials for photovoltaic (PV) systems. The materials are abundant on the planet, non-toxic, and inexpensive. In this work, CZTS and CZTSe were synthesized by using two techniques. Firstly, copper zinc tin sulfide and selenide CZTS and CZTSe thin films have been prepared using two-step procedure. The initial step started with the preparation of $\text{Cu}_2\text{ZnSnS}_4$ and $\text{Cu}_2\text{ZnSnSe}_4$ powder using the melt quenching technique, and the second step is the fabrication of CZTS and CZTSe thin films using the thermal evaporation deposition process. The obtained films were heat-treated at annealing temperatures of 50, 150, and 300°C. UV. Vis spectroscopy, Atomic force microscopy (AFM), Field emission scanning electron microscopy (FE-SEM), X-ray diffraction (XRD), and Fourier transform infrared (FTIR) spectroscopy were used to characterize the samples. The XRD result showed that crystal structure of all of the films were polycrystalline kesterite phase. At 300 °C, CZTS film crystallite size was (9.8 nm) and for CZTSe film was (10.9 nm). The direct band gaps for CZTS and CZTSe estimated by Tauc's equation were (1.95 and 1.89 eV); (1.90 and 1.79 eV); (1.87 and 1.71 eV) at 50, 150, and 300°C. The energy gap of CZTS and CZTSe materials is not far off the optimum value for the greatest solar cell efficiency. According to AFM findings, particle size and root-mean-square (RMS) of CZTS and CZTSe film increased with increasing annealing temperature when grain size is directly related to temperature. In addition, the surface morphological characteristics showed smooth, compact and uniform film formation at highest annealing temperature. The functional groups are analyzed by using FTIR spectroscopy. Hall measurements revealed that all of the samples were p-type. The highest carrier concentrations were found $9.75 \times 10^6 \text{ cm}^{-3}$ for CZTS at 300°C and $6.72 \times 10^6 \text{ cm}^{-3}$ for CZTSe at the same temperature. The

maximum open-circuit voltage (V_{OC}) was 0.23 mV, the highest short-current density (J_{SC}) was 7.41 mA/cm², and the highest efficiency (η) was 14.8%, according to measurements of heterojunction for ITO/CZTS/CdS/ZnO/Al solar cell devices' (J-V) curves; as for ITO/CZTSe/CdS/ZnO/Al solar cell devices, were the highest open-circuit voltage (V_{OC}) 0.38 mV and short-current density (J_{SC}) 4.9 mA/cm², and the device highest efficiency (η) was 15.6 %, therefore, both devices went through an annealing process at 300 °C

Secondly CZTS and CZTSe thin films have been prepared using a two-step procedure. The initial step started with the preparation of CZTS and CZTSe powder using the hydrothermal technique which was heat-treated at annealing temperatures of 400, 600, and 800°C, whereas the second step is the fabrication of CZTS and CZTSe thin films using a spin coating process. AFM, FE-SEM, XRD, and FTIR were used to characterize the samples. The XRD result showed that the crystal structure of all films was polycrystalline kesterite phase. At 800 °C, CZTS film crystallite size was (15.47nm) and for CZTSe film was (25.4nm). The morphological properties using FE-SEM showed that the CZTS and CZTSe thin films shape were compact with more densely packed grains at the highest annealing temperature. According to AFM results, particle size and (RMS) of CZTS and CZTSe film increased with increasing annealing temperature when grain size is directly associated with temperature. The direct band gaps for CZTS and CZTSe estimated by Tauc's equation were (1.73 and 1.68) eV; (1.66 and 1.59) eV; (1.56 and 1.53) eV at 400°C, 600°C, and 800°, the energy gap of CZTS and CZTSe materials is not far off the optimum value for greatest solar cell efficiency. Hall measurements revealed that all of the samples were p-type. The lowest value of resistivity was found to be 0.031 Ω .cm for CZTS at 800°C and 0.0191 Ω .cm for CZTSe at the same temperature. The maximum open-circuit voltage (V_{OC}) was 0.39 mV, the highest short-current density (J_{SC}) was 4.81 mA /cm², and the highest

efficiency (η) was 13.3%, according to measurements of heterojunction for ITO/CZTS/CdS/ZnO/Al solar cell devices' (J-V) curves; as for ITO/CZTSe/CdS/ZnO/Al solar cell devices, were the highest open-circuit voltage (V_{OC}) 0.42 mV and short-current density (J_{SC}) 5.12 mA/ cm², and the device highest efficiency (η) was 15.1 %, therefore, both devices went through an annealing process at 800 °C.

Table of Contents

Subject	Page No.
Table of Contents	I
List of Abbreviations	VII
List of Symbols	VIII
List of Figures	X
List of Tables	XIII

Table of Contents

Item No.		Page No.
Introduction & Literature Review		
1.1	Introduction	1
1.2	Generation solar cells	3
1.2.1	First-generation solar cells	3
1.2.2	Second-generation solar cell	3
1.2.3	Third-generation solar cells	4
1.3	The Novel Material: CZTS and CZTSe	5
1.4	Literature review	6
1.5	Aims of the work	14

Chapter Two: Theoretical Part		
2.1	Introduction	15
2.2	Solar cells	15
2.2.1	Solar spectrum	15
2.2.2	Absorption of light	17
2.2.3	p-n junction under equilibrium	19
2.2.3.1	p-n junction under biases	20
2.2.3.1.1	Forward bias	20
2.2.3.1.2	Reverse bias	21
2.2.3.2	p-n junction under illumination	22
2.2.3.3	Junctions in semiconductors	25
2.2.4	Solar cell parameters	26
2.2.4.1	Open circuit voltage (V_{oc})	27
2.2.4.2	Short circuit current density (J_{sc})	28
2.2.4.3	Fill Factor (FF)	28
2.2.4.4	Efficiency (η)	28
2.2.5	Equivalent circuit of solar cells	29
2.2.5.1	Series resistance (R_s)	29
2.2.5.2	Shunt resistance (R_{sh})	30

2.3	CZTS and CZTSe solar cell technology	31
2.3.1	Application of CZTS and CZTSe in Solar Cells	32
2.3.1.1	Device structure and basic working principles	32
2.3.1.2	Copper Zinc Tin Sulphide CZTS	33
2.3.1.3	Copper Zinc Tin Selenide CZTSe	34
2.4	The crystal structure of CZT(S, Se)	34
2.4.1	Optical energy gap of CZTS and CZTSe	36
2.4.2	Structure of thin film	36
2.5	CZTS secondary phases and ternary phase structure	37
2.6	CZTSe secondary phases and ternary phase structure	38
2.7	Synthesis of CZTS and CZTSe powders	39
2.7.1	Melt quench technique	39
2.8	Hydrothermal synthesis	40
2.8.1	Hydrothermal chemistry	40
2.9	Fabrication of CZTS and CZTSe absorber layer	43
2.9.1	Vacuum based deposition process	43
2.9.2	Non-Vacuum based process	43
Chapter Three: Experimental Procedure		
3.1	Introduction	46

3.2	Experimental work	46
3.3	Materials	47
3.4	Preparation of CZTS and CZTSe powder by melt quenching technique	48
3.5	Thin film deposition	50
3.5.1	Substrates cleaning	50
3.5.2	Thermal evaporation deposition technique	51
3.6	Preparation CZTS and CZTSe powder by hydrothermal technique	52
3.6.1	Preparation of CZTS nanoparticle powder	52
3.6.2	Preparation of CZTSe powder	53
3.7	Thin film deposition	53
3.7.1	Spin coating technique	53
3.8	Preparation of multijunction solar cells	53
3.8.1	Back contact	53
3.8.2	Absorber layer	54
3.8.3	Buffer layer	54
3.8.4	Window layer	54
3.8.5	Counter electrode (Al) deposition	55
3.9	Measurements	55

3.9.1	X-Ray diffraction (XRD)	55
3.9.2	Field emission scanning electron microscopy(FESEM)	56
3.9.3	UV-Vis Spectroscopy	56
3.9.4	Fourier Transform-Infrared Spectroscopy (FTIR)	56
3.9.5	Atomic force microscopy (AFM)	57
3.9.6	Hall effect	57
3.9.7	Optical interference method	57
3.9.7	Current-Voltage (I-V) measurement system	57
Chapter Four Results & Discussion		
4.1	Introduction	58
4.2	Result measurements of CZTS and CZTSe quaternary compounds thin films by using melt quenching and PVD technique	58
4.2.1	XRD analysis of CZTS and CZTSe powders	59
4.2.2	XRD analysis of CZTS and CZTSe thin films	60
4.2.3	XRD analysis of ZnO and CdS thin films	64
4.2.4	FTIR analysis results	66
4.2.5	Atomic force microscope (AFM)	67
4.2.6	Field emission scanning electron microscopy	70

4.2.7	The Optical Properties results	75
4.2.8	Electrical properties	77
4.2.9	J-V Characterizations of CZTS and CZTSe quaternary compounds (ITO/CZTS/CdS/ZnO) and (ITO/CZTSe/CdS/ZnO) Solar Cells	78
4.3	Formation of quaternary compounds CZTS and CZTSe by using hydrothermal synthesis and spin coating technique	81
4.3.1	X-ray diffraction (XRD) analysis of CZTS and CZTSe) powders	81
4.3.2	X-ray diffraction (XRD) analysis of CZTS and CZTSe thin film result	82
4.3.3	FTIR analysis result	87
4.3.4	Atomic force microscope (AFM) result	88
4.3.5	Field-emission scanning electron microscopy (FE-SEM) result	91
4.3.6	The Optical Properties result	93
4.3.7	Electrical properties result	95
4.3.8	J-V characterizations of CZTS and CZTSe quaternary compounds ITO/CZTS/CdS/ZnO/Al and ITO/CZTSe/CdS/ZnO/Al solar cells	96
4.4	Comparative study	99
4.5	Conclusions	100
4.6	Future Works	101

	References	102
	Appendices	

List of Abbreviations

Abbreviation	Definition
AM	Air Mass
AM0	The solar radiation spectrum outside of the earth's Atmosphere
AM1	The distance of the solar radiation spectrum required to reach the earth's surface when the sun is directly at an overhead position relative to the earth
AM1.5	Solar radiation at the earth's surface when the solar rays make an angle of 48.2° with the vertical
4GSCs	Fourth Generation Solar Cells
CZTS	Copper zinc tin sulfide
CZTSe	Copper zinc tin selenide
a-Si	Amorphous Silicon
CB	Conduction Band
CIGS	Copper Indium Gallium Selenide
c-Si	Crystalline Silicon
LEDs	light emitting diodes
DIW	Deionized water
CdTe	Cadmium Telluride
DSSCs	Dye Sensitized Solar Sells
FESEM	Field Emission Scanning Electron Microscopy

ITO	Indium Tin Oxide
FWHM	Full Width at Half Maximum
I-V	Current-Voltage
J-V	Current density–Voltage
MA	Methyl amine
MPP	Maximum Power Point
PCE	Power Conversion Efficiency
PV	Photovoltaic
TCO	Transparent Conductive Oxide
UV-Vis	Ultraviolet-Visible
XRD	X-Ray Diffraction
ICDD	International Center for Diffraction Data

List of Symbols

Symbol	Meaning	Units
A	Absorbance	-
a,b and c	Lattice constants	Å
c	Speed of light	m/s
D	The crystallite size	nm
d_{hkl}	Interplanar spacing	Å
E	Energy of the photon	eV
E_g	Optical Energy Gap	eV

FF	Fill Factor	-
hkl	Miller indices	-
I_{ph}	The light-generated current density	mA
I_{SC}	Short circuit current	mA
I_{Sh}	Shunt current	mA
J_{max}	Current density at maximum power point	mA/cm ²
J_{SC}	Short-circuit current density	mA/cm ²
K_B	Boltzmann constant	J/K
B	Constant	-
η	Efficiency	-
P_{in}	The incident power	mW/cm ²
P_{max}	Maximum power	mW/cm ²
q	The electron charge	-
T	The temperature	K
V_{max}	Maximum voltage	V
V_{OC}	Open-circuit voltage	V
α	Optical absorption coefficient	cm ⁻¹
θ_z	Solar zenith angle	Degree
λ	Wavelength of the photon	nm
n	Integer number	-
A	The active surface area of the cell	cm ²
K	Scherrer's constant	-

θ	Bragg's angle	degree
β	Full width at half maximum	rad
R_s	Series resistance	$\Omega.cm^2$
R_{Sh}	Shunt resistance	$\Omega.cm^2$

List of Figures

Fig. No.	Figure Caption	Page No.
1.1	Comparison of the costs and availability of major components used in the production of thin film solar cells	2
1.2	The classification of solar cells	4
2.1	Spectra of a solar cell spectrum at AM0 and AM1.5	16
2.2	(a) The GaAs direct bandgaps, whereas (b) shows the Si indirect bandgap, (c) CZTS direct bandgaps	17
2.3	p-n junction	19
2.4	Effect of forward bias on the depletion region in a p-n junction	21
2.5	Effect of Reverse bias on the depletion region in a p-n junction	21
2.6	The Ohmic and Schottky junctions for a p-type semiconductor	26
2.7	The J-V curve in both dark and illuminated conditions	27
2.8	Solar cell equivalent circuit	29
2.9	The effect of series resistance	30
2.10	The effect of shunt resistance	30

2.11	The configuration of CZTS solar cell	33
2.12	Depictions of unit cells of (a) kesterite and, (b)stannite type structures. Zn atoms are depicted in yellow, while Cu atoms are shown in blue and Sn atoms in red. The anions are depicted as large, pale yellow spheres	35
2.13	Ternary phase diagram of CZTS	37
2.14	Pseudo-ternary phase diagram of CZTSe	39
2.15	The schematic of a hydrothermal synthesis apparatus	41
2.16	Dielectric constant of water changes as a function of temperature and pressure	42
2.17	Steps of spin coating on substrate	44
2.18	The steps involved in coating a kesterite layer with a direct solution	45
3.1	Schematic diagram of the experimental work	46
3.2	Schematic diagram of CZTS and CZTSe preparation steps by melt quenching technique	48
3.3	(a)Schematic diagram of the thermal evaporation system used. (b) Photographs of the thermal evaporation	51
3.4	Schematic diagram of CZTS preparation steps by hydrothermal technique	52
3.5	a. solar cell devices, b. Schematic diagram of shadow mask.	55
3.6	Schematic diagram of (I-V) measurement system	58
4.1	XRD patterns of CZTS powder	59
4.2	XRD patterns of CZTSe powder	59
4.3	XRD patterns of CZTS thin films synthesized at different annealing temperatures (50, 150, and 300) °C.	61

4.4	XRD patterns of CZTSe thin films synthesized at different annealing (50, 150, and 300) °C.	61
4.5	XRD patterns of ZnO thin film	65
4.6	XRD patterns of CdS thin film	65
4.7	FTIR spectrum of CZTS powder	66
4.8	FTIR spectrum of CZTSe powder	67
4.9	AFM images of CZTS thin films at different annealing temperatures (a) 50, (b) 150 and (c) 300 °C.	68
4.10	AFM images of CZTSe thin films at different annealing temperatures (a) 50, (b) 150 and (c) 300 °C.	69
4.11	FE-SEM images of CZTS thin films, annealed at (a) 50, (b) 150 and (c) 300 °C	70
4.12	FE-SEM cross section images of CZTS thin films, annealed at (a) 50, (b) 150 and (c) 300 °C	71
4.13	FE-SEM images of CZTSe thin films, annealed at (a) 50, (b) 150 and (c) 300 °C	72
4.14	FE-SEM cross section images of CZTSe thin films, annealed at (a) 50, (b) 150 and (c) 300 °C.	73
4.15	Energy-dispersive X-ray spectroscopy of CZTS thin film that were prepared at 300 °C	74
4.16	Energy-dispersive X-ray spectroscopy of CZTSe thin film that were prepared at 300 °C.	74
4.17	Tauc's plots of CZTS thin films annealed at different annealing temperatures	76
4.18	Tauc's plots of CZTSe thin films annealed at different annealing temperatures.	76
4.19	J-V characteristic of CZTS heterojunction solar cells	79
4.20	J-V characteristic of CZTSe heterojunction solar cells	80
4.21	X-ray diffraction patterns of CZTS powder	81

4.22	X- ray diffraction patterns of CZTSe powder	82
4.23	X- ray diffraction patterns of CZTS thin films synthesized at different calcinating temperatures (400, 600 and 800) °C.	83
4.24	X- ray diffraction structures of CZTSe thin films synthesized at different calcinating temperatures (400, 600 and 800) °C.	84
4.25	FTIR Spectrum of CZTS	87
4.26	FTIR Spectrum of CZTSe	88
4.27	3-D AFM images of CZTS with calcinating (a) 400°C, (b) 600°C and (c)800°C thin films.	89
4.28	3-D AFM images of CZTSe with calcinating (a) 400°C, (b) 600°C and (c)800°C thin films.	90
4.29	FE-SEM images of CZTS thin films calcinated for (a) 400, (b) 600 and (c) 800 °C.	91
4.30	FE-SEM images of CZTSe thin films calcinating for (a) 400, (b) 600 and (c) 800 °C.	92
4.31	Tauc's plot of CZTS thin film	93
4.32	Tauc's plot of CZTSe thin film	94
4.33	J-V characteristic of CZTS heterojunction solar cells	97
4.34	J-V characteristic of CZTSe heterojunction solar cells	98

List of Tables

Table No.	Table caption	Page No.
3.1	The materials used to prepare solar cells	47
4.1	XRD results of prepared CZTS thin films at annealing temperatures (50,150,300) °C	62
4.2	XRD results of prepared CZTSe thin films at annealing temperatures (50,150,300) °C	63

4.3	XRD results of prepared CZTS and CZTSe thin films at different annealing (50 °C, 150 °C and 300 °C)	64
4.4	Surface roughness, root mean square (RMS) surface roughness and grain size of CZTS and CZTSe thin films at different annealing temperatures	69
4.5	Weight and atomic percentages of the elements for CZTS thin film that were prepared at 300 °C	75
4.6	Weight and atomic percentages of the elements for CZTSe thin that were prepared at 300 °C	75
4.7	Hall effect properties of CZTS and CZTSe films deposited with different annealing temperatures	77
4.8	The photovoltaic parameters results of the solar cells fabricated by using melt	80
4.9	X-RAY diffraction results of prepared thin films at annealing temperatures (400,600,800) °C	85
4.10	XRD results of prepared CZTSe thin films at annealing temperatures (400,600,800) °C	86
4.11	XRD analysis of CZTS and CZTSe at different annealing temperatures (400, 600, and 800) °C.	86
4.12	Surface roughness, root mean square (RMS) surface roughness and grain size of CZTS and CZTSe thin films at different calcinating temperatures.	90
4.13	Hall effect properties of CZTS and CZTSe films deposited using different annealing	95
4.14	The photovoltaic parameters result of the solar cells fabricated by using Hydrothermal	96
4.15	Comparative analysis of different methods for CZTS and CZTSe thin-film formation and solar cell application	99

Chapter One

Introduction &

Literature review

1.1 Introduction

More than 80% of the world's energy is currently produced from fossil fuels like coal, oil, and natural gas. These fuels produce greenhouse gases when they are consumed. In addition, the cost of the energy generated by these sources is rising. All of the world's energy needs can be met by photovoltaic (PV) energy, which is abundant, clean, and non-polluting. Electronic devices that convert sunlight into power are known as solar cells. To supply the world's energy needs, we only need to cover 0.1 percent of the earth's surface with 10 percent power conversion efficiency (PCE) solar cells [1]. At the moment, the high costs of solar cell production and construction are preventing widespread use of the technology [2]. The most common type of solar cell is made from crystalline silicon, which is extremely pure. The cost of solar panel production is pushed up by the high cost of silicon fabrication. As a feasible alternative to silicon-based solar cells, thin-film solar cells are rising in popularity. When it comes to absorption, a 100 times thinner layer of thin film absorber materials may absorb the same amount of energy as crystallized silicon, which has a 100 times greater absorption coefficient. Because the grain boundaries in thin film materials make it easier to separate charges and convey them while also allowing for less recombination, they are less critical in film solar cell materials than they are in crystalline silicon solar cells [3]. To put it another way, thin-film solar cells are less expensive to produce than silicon solar cells.

Thin-film solar cells are catching on as a practical replacement for silicon-based solar cells. Instead of using thin semiconductor films like cadmium telluride (CdTe) or copper indium gallium diselenide, these devices utilize thick silicon wafers (CIGS). Because of the toxic or scarce nature of many of the semiconductor elements commonly used in their production (such as cadmium), film solar cells

made from CIGS and CdTe have already achieved astounding laboratory efficiency of around 15-20 percent (like, indium, tellurium). Cost and availability of various materials are shown in Figure 1.1. These solar cells are only viable if they use non-toxic and abundant materials that can be found on Earth.

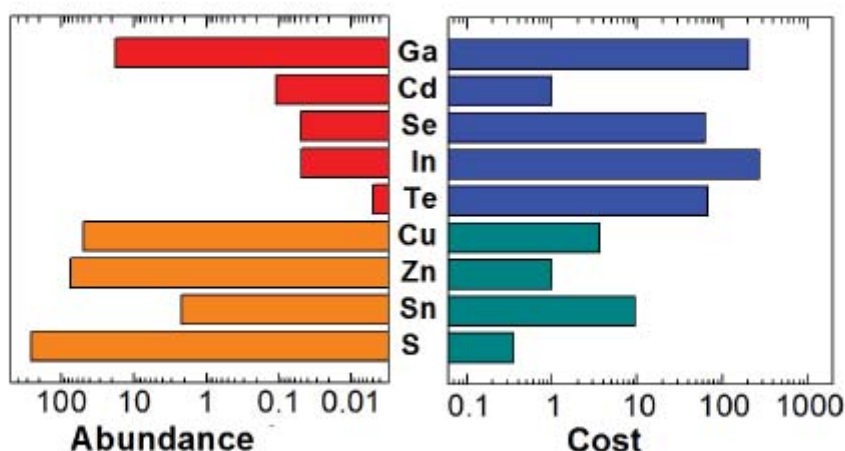


Figure 1.1: Comparison of the costs and availability of major components used in the production of thin film solar cells [4].

By the way, the quaternary compounds such as $\text{Cu}_2\text{ZnSnS}_4$ (CZTS) and $\text{Cu}_2\text{ZnSnSe}_4$ (CZTSe), due to their appropriate optical characteristics, elemental availability, and nontoxicity of their elements, are emerging as viable active-layer semiconductor for low-cost thin-film solar cell applications [5]. In the literature, CZTS refers usually to the selenide, sulfide, or sulfide-selenide form of the compound. CZTS and CZTSe compounds are p-type semiconductors with a direct bandgap of nearly 1.5 (eV) for selenide (CZTSe) [6] and about 1.6 eV for sulfide (CZTS) [7].

There have been numerous published research on the production of CZTS even though it is a relatively new material. This includes both vacuum and non-vacuum procedures. CZTS and CZTSe devices with an active layer manufactured using solution-based methods have the highest PCE of 8.4%, while CZTS devices

with a thermally evaporated CZTS absorbent layer have the highest PCE of 12.6 percent [9]. However, despite significant progress toward improved PCEs for CZTS-based solar cells, the best-reported device's performance remains far below the theoretically predicted efficiency of roughly 30% [10].

1.2 Generations of solar cells

1.2.1 First-generation solar cells

The photovoltaic effect was discovered in 1839 [11], despite this, the first silicon (Si) p-n junction structured PV device was invented by Bell laboratories in 1954 [12]. Crystalline silicon was the primary material used in the first wave of solar cell development because of its ubiquitous availability. Based on the degree of crystallization, first-generation solar cells can be split into two groups. A monocrystalline solar cell has only one crystal, and a polycrystalline solar cell which has several crystals in it. Other absorber materials for PV devices, notwithstanding Si market dominance, are also being researched. Device manufacturing requires an enormous amount of silicon, which has a wide range of pricing, as well as significant material processing expenses [13].

1.2.2 Second-generation solar cell

The light absorber in second-generation solar cells is more effective at absorbing light than in first-generation solar cells, therefore they utilize less material. Because they are substantially thinner than crystalline silicon solar cells, second - generation solar cells are often referred to as thin film solar cells. Cu(In, Ga)Se₂ (CIGS), CdTe, and amorphous silicon (a-Si) are the most commonly utilized thin film light absorber materials. Compared to the absorber layers of silicon-based solar cells, the CdTe and CIGS absorber layers are typically 10 μm and 2.5 μm in thickness, respectively [14,15]. Cell efficiencies of 20.4% and 19.6%, have been obtained in CIGS and CdTe respectively [16], edging closer to

monocrystalline silicon's all-time high (25.0 percent) [17,18]. However, the scarcity of In, Ga, and Te rare metals has resulted in a higher production cost because of their limited availability. CIGS and CdTe-based PV devices currently account for 10 to 15 percent of the market, following Si solar cells [19].

1.2.3 Third-generation solar cells

A high power conversion efficiency and low cost make third-generation solar cells ideal. As a result, the production cost is heavily influenced by the amount, accessibility, and ease with which materials used in device creation may be processed. A wide range of cutting-edge technologies and materials have been employed in the development of 3rd generation solar cells. Solution-processed photovoltaic devices, such as sensitized solar cells, $\text{Cu}_2\text{ZnSnS}_4$ and $\text{Cu}_2\text{ZnSnSe}_4$, and polymer organic solar cells, have numerous applications due to their low manufacturing costs. CZTS and CZTSe are the most promising light absorber materials for next-generation thin-film PV because of its low raw material cost and toxicity [20]. Figure (1.2) shows the classification of solar cells.

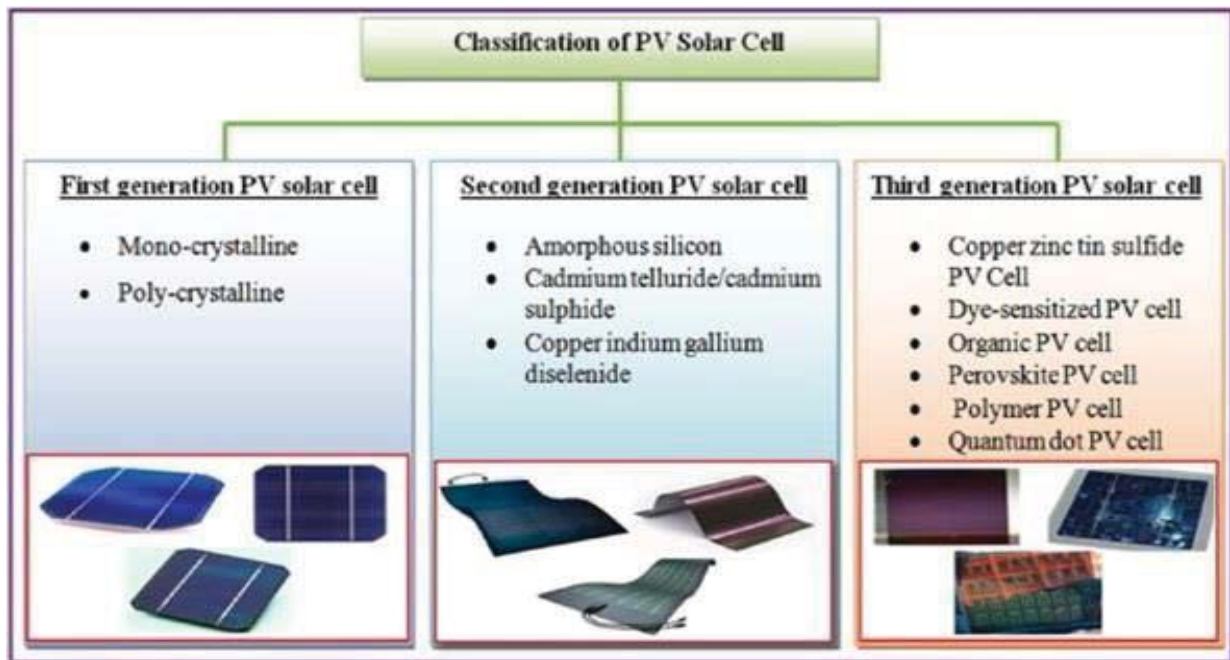


Figure 1.2: The classification of solar cells [21].

1.3 The Novel Material: CZTS and CZTSe

The potential uses of copper chalcogenide semiconductors in photovoltaics (PV), photocatalysis, solid-state light-emitting diodes (LEDs), and biomedicine have sparked a lot of interest in the past [22]. Due to their optical absorption coefficient, photo stability, low cost, and desirable direct bandgaps, CZTS and CZTSe copper-based quaternary compounds have attracted attention. CZTS and CZTSe are being researched as an alternative light absorption material to CIGS and CdTe [23] because the production cost can be further reduced and production scale restrictions can be overcome. Copper (Cu), zinc (Zn), tin (Sn), sulphur (S), and selenium (Se) are the only elements in CZTS and CZTSe that are readily available [24], inexpensive, and kind to the environment. For example, zinc and tin are all more abundant than indium and gallium [25].

1.4 Literature Review

Tiwari et al. (2014) deposited CZTS thin film by using sol-gel by spin-coating technique. The replacement reaction route is used to prepare the CZTS thin film. The soda lime glass substrate was coated with a ZnS layer using chemical Bath deposition (CBD) in this procedure. Once this was done, it was submerged in a metal solution containing cupric chloride, zinc chloride, and stannous chloride for 10 minutes, and then the glycerol solution was added. Sol-gel spin coating was used to deposit ZnO onto an ITO coating on SLG for use in solar cells. CBD was then used to deposit CdS. Colloid graphite served as a top contact after the CZTS was deposited using the replacement reaction route. AFM indications the films to be homogeneous and compact with RMS roughness of 6 nm. The direct band gap of CZTS films was 1.45 eV. The CZTS films exhibit p-type conduction, the hole concentration and hole mobility is determined to be $3.6 \times 10^{17} \text{ cm}^{-3}$ and $1.4 \text{ cm}^2\text{V}^{-1}$

s⁻¹ respectively. With a superstrate configuration of graphite/ CZTS/ CdS/ ZnO/ ITO/ SLG, the solar cells produced $V_{oc} = 521$ mV, $J_{sc} = 19.13$ mAcm⁻², FF = 62%, and 6.17 percent efficiency [26].

Bakr et al. in 2015 prepared copper zinc tin sulfide (CZTS) films by using chemical spray pyrolysis technique at temperatures ranging from 200°C to 450°C on clean, preheated glass substrates. Scherrer's formula was used to calculate the crystallite size. The XRD results showed that all films are polycrystalline in nature with tetragonal structure and preferred orientation along (112) plane. AFM results showed homogenous and smooth thin films. The absorbance and transmittance spectra have been recorded in the wavelength range of (300- 900) nm. And Tauc's equation was used to calculate the optical energy gap for direct electronic transition. This study found that as the substrate temperature increases, the band gap decreases and the optical allowed energy gap for the direct electronic transitions ranged from (2.3 -1.85) eV [27].

Mrzog in 2015 investigated how changing the electrochemical deposition parameters affected the characteristics and development of CZTS thin films. When the triangle wave pulse affects the characteristics of CZTS thin films. It was found that the energy band gap (E_g) about 1.48 eV, the concentration and the mobility of CZTS films were 4.5×10^{20} cm⁻³ and 3.79 cm² V⁻¹S⁻¹, The efficiency of the solar cell with a device glass/Mo/CZTS/CdS/ZnO/Al:ZnO/ was 2.94% [28].

Bakr et al. in 2016 deposited Cu₂ZnSnS₄ (CZTS) thin films by using chemical spray pyrolysis (CSP) technique at substrate temperature of (400) °C and of about (300) nm thickness at different thiourea concentrations of (0.14,0.16, 0.18, 0.20, 0.22 and 0.24) M. It was found that the energy band gap (E_g) decreases as the

thiourea concentration increases and it was in the range of (2.22 - 1.75) eV. The XRD results showed that all films are polycrystalline in nature with tetragonal structure and preferred orientation along (112) plane. The AFM results showed smooth and homogenous thin films [29].

Qu et al. in 2016 synthesized $\text{Cu}_2\text{ZnSnS}_4$ (CZTS) nanoparticle inks and the influence on the performance of thin film solar cells made by converting the nanoparticles to large CZTSSe grains in selenium has been investigated. The reaction time, temperature and cooling rate of the nanoparticle fabrication process are found to affect doping level, secondary phases and crystal structure respectively [30].

Das et al. in 2018 investigated $\text{Cu}_2\text{ZnSnS}_4$ (CZTS) thin films as their non-toxicity, earth-abundant nature, and ideal band gap matched with solar spectrum (1.45- 1.65eV), thin films are a viable absorber for inorganic photovoltaic device application, high absorption coefficient (10^4cm^{-1}). Structure, phase, and shape of produced CZTS nanocrystals have been verified by XRD, SEM, and other characterization techniques. The crystalline phase of synthesized CZTS has been confirmed by X-ray diffraction analysis. Nanocrystals of CZTS are typically around 4 nm in size. In a photovoltaic device, the synthetic CZTS nanocrystals could serve as the absorber layer. Here, a low cost, environment friendly facile hydrothermal route to synthesize phase pure CZTS nanoparticles [31].

Fouad et al. in 2018 Using a low-cost chemical bath deposition process, generated high-quality $\text{Cu}_2\text{ZnSnS}_4$ thin films of various thicknesses (240-418) nm were deposited on previously cleaned glass substrates. The impact of the deposition circumstances on the variation of the CZTS films' structural, optical, optoelectrical, and electrical properties has been studied. The XRD shows CZTS

thin films exhibited a polycrystalline the kieserite crystal structure. The difference of the DC conductivity with temperature for the CZTS thin films. An Al/n-Si/P-CZTS/Au hetero-junction has been created. The substrate for the device was a 0.5 mm thick, 1-10 Ω .cm resistive, phosphorus-doped Si wafer. Photovoltaic behavior was observed for the fabricated device which had a solar conversion efficiency of 3.37% [32].

Chang et al. in 2018 studied the effects of heat treatment on the efficiency of $\text{Cu}_2\text{ZnSnS}_4$ solar cell. Solar cells with an ($V_{oc} = 730$ mV) and PCE of 11% were found using heat treatment to decrease heterojunction recombination. When Cd atoms are exposed to this heat treatment, they are more easily moved into Zn or Cu lattice sites, the performance improvement of CZTS photovoltaic is achieved by using a simple heterojunction heat treatment process. This approach enables elemental inter diffusion, leading to a Zn gradient within CdS and a Cd gradient within CZTS, as well as a Na accumulation and local Cu-depletion at the heterojunction. The approach also leads to the formation of new phases: Cd diffusion into the lattice of CZTS surface forms a thin layer of $\text{Cu}_2\text{Cd}_x\text{Zn}_{1-x}\text{SnS}_4$ while Zn diffusion into the CdS likely forms ultrathin $\text{Zn}_x\text{Cd}_{1-x}\text{S}$; and likely formation of a new phase of $\text{Cu}_{2-x}\text{Na}_x\text{ZnSnS}_4$ (average $x \sim 0.07$) nanoclusters are revealed. The allowing for greater elemental inter-diffusion. This, in turn, promotes Na accumulation and local Cu deficiency within the heterojunction region. A better alignment of the conduction bands is obtained near the hetero-interface, resulting in new phases forming and reducing non-radiative recombination. The first kesterite cell (including selenium-containing) of standard centimeter-size to surpass 10% efficiency was demonstrated using this approach, and it was certified at a centimeter-scale (1.11 cm^2) of 10 percent $\text{Cu}_2\text{ZnSnS}_4$ [33].

Cui et al. in 2018 created a variety of $Zn_{1-x}Sn_xO$ (ZTO, $0 \leq x \leq 1$) films using atomic layer deposition for use as a buffer layer in CZTS photovoltaic cells. A 10 nm $Zn_{0.77}Sn_{0.23}O$ buffer layer is used to establish a good band alignment, which led to an astonishing 10% rise in the V_{oc} of the CZTS solar cell. The existence of an incredibly thin Zn(S, O) layer is proven by meticulous examination of the microstructure and chemical makeup of the CZTS/ZTO interface. The large improvement in open circuit voltage is explained by the lowered interfacial defects resulting from the slight lattice mismatch at the CZTS/Zn(S,O)/ZTO heterointerface, as well as the passivation given by a greater sodium concentration throughout the CZTS/ZTO device. They concluded by demonstrating a CZTS solar cell efficiency of 9.3%, the best efficiency for a Cd-free pure sulphide CZTS solar cell [34].

Zhang et al. in 2019 fabricated CZTS nanocrystal inks by a wet ball milling method. The as-fabricated CZTS nanocrystal inks were used to deposit CZTS precursors with precisely controlled CZTS films by a spin-coating method followed by a rapid high pressure sulfur annealing method. XRD and Raman characterization showed no secondary phases in the annealed film, the absence of the detrimental phases. A solar cell efficiency of 6.2% ($V_{oc} = 633.3$ mV, $J_{sc} = 17.6$ mA/cm², and FF = 55.8%) with an area of 0.2 cm² was achieved based on the annealed CZTS film as the absorber layer [35].

Mkawi et al. in 2019 studied the effects of morphological, structural and electrical characteristics of the synthesized structures. Analytical methods were used to determine the composition of the samples. These nanoparticles have a kesterite structure according to XRD patterns and Raman measurements. Spherical CZTS nanoparticles can be seen forming using transmission electron microscopy in oleylamine (OLM) of 6 mL. Examination of the nanocrystal thin films by

scanning electron microscopy reveals a perfect, uniform-grain structure with particle sizes between 1 and 2 μm . The direct band gap measured in UV-Vis-NIR spectra was 1.47 eV, putting it on the cusp of the ideal value needed for photovoltaic applications. There is commercial potential for the synthetic method because of its speed and ease of use. The conversion efficiency of solar cells constructed from glass/Mo/CZTS/CdS/i-ZnO/AZO/Ag was determined to be around 2% [36].

Mkawi in 2020 examined how several metals (Li, Na, Sb, and Cr) affected the characteristics of CZTS thin films. The structural, morphological, electrical, and optical properties of the films were examined. Using electrodeposited thin films, he showed the spin coating process for the deposition of four distinct metals. After doping, the crystallinity of the kesterite phase improved, and X-ray diffraction (XRD) corroborated this. The major intensity peaks of the kesterite phase correspond to the (112), (200), (312), and (332) planes. The Na-doped CZTS thin film contained a pure kesterite phase with just a small quantity of contaminants, according to Raman spectroscopy. Based on the absorption measurements, an energy gap absorption edge with a range of (1.56 - 1.71) eV was estimated, and depending on the doping metal, improvements in the energy gap were seen. In the visible spectrum of light, the absorption coefficient exceeded 10^4 cm^{-1} . Under simulated AM1.5, the solar cell's performance was 2% when its device configuration was Glass/ITO/CZTS/CdS/i-ZnO/ZnO: Al/Ag [37].

Mkawi et al. in 2020 studied the effects material properties while controlling the size of $\text{Cu}_2\text{ZnSnS}_4$ nanoparticles by means of XRD (X-ray diffraction), UV-Vis (spectroscopy), electron microscopy (FE-SEM), and Raman spectroscopy, as well as by means of TEM (electron microscopy). The high crystallinity of the kesterite phase was confirmed by XRD and Raman spectroscopy. An obvious

preferential orientation of the nanoparticles was found to be along a crystallographic axis (112). It was found that CZTS nanoparticles have a bandgap between 1.59 eV and 1.82 eV, which is close to the optimum bandgap value for solar cell conversion devices, according to UV-Vis absorption measurements. CZTS nanoparticle crystals with diameters ranging from 10 to 40 nm were found in the TEM study, depending on the concentration of the stabilizing agent. In solar cell devices utilizing Al/ZnO: Al/ZnO/CdS/CZTS/Mo, the CZTS synthesized with PVP stabilizer at a concentration of 9 mg/mL had a maximum $J_{sc} = 9.83$ mA per cm^2 , $V_{oc} = 0.453$ V, F.F = 61.1 percent, and an efficiency of 2.7% for Al/ZnO [38].

Chamekh et al. in 2020 Cu_2ZnSnS_4 (CZTS) thin films' structural and optical properties were studied, where the films were annealed at different temperatures. Vacuum thermal evaporation was used to deposit thin films onto regular glass substrates. CZTS film structure was analyzed by means of the Diffraction by X-rays. The spectra demonstrated that the crystalline quality of CZTS films was improved by heat treatments. In all annealed films, it was discovered that the (112) direction was the favored orientation. features of optoelectronics CZTS thin films were investigated using UV-Vis spectrophotometry. Optical analysis of annealed specimens showed a coefficient of absorption greater than 10^4 cm^{-1} band gap between 1.48 and 1.56 eV [39].

Tikote et al. in 2020 studied a simple hydrothermal synthesis route for quaternary kesterite CZTS powder without any post annealing treatment. The effect of reaction temperature on the properties of CZTS was investigated. The sample obtained at high reaction temperature 200°C revealed the formation of pure CZTS, tetragonal structure with (112), (220) and (312) reflections, while for low

reaction temperature various secondary and ternary phases were observed. The Raman result agreed well with the structural analysis reported using XRD. The energy band gap $\sim 1.50\text{eV}$ was estimated for the sample prepared at higher reaction temperatures. Stoichiometric chemical composition of CZTS sample (2:1:1:4) was determined for the sample synthesized at 200°C [40].

Ozidal et al. (2020) examined the influence of annealing temperature on CZTS thin films using the sol-gel spin coating process, they looked at the morphology and optoelectronics properties. The achieved results for X-ray diffraction (XRD) indicated a polycrystalline structure of CZTS thin film, the SEM and AFM micrographs showed a uniform and dense texture of the samples, besides the effect of annealing temperatures on CTZS morphology and surface was discussed. Eg of the films annealed at 300, 500 and 550°C was found to be 1.58 eV and 1.63 eV for film annealing 400°C [41].

Vishvas et al. in 2021 examined thermal evaporation-deposited CZTSe films. After deposition, the films underwent a 10 min annealing process at 450°C . After being deposited and annealed, the films were treated with thiourea solution to add sulphur and partially replace the Se (1 Molar). The films were additionally annealed for 10 minutes at 450°C following the thiourea treatment. The films were characterized for phase analysis using XRD, and crystallite size was discovered (11.7 – 16.74) nm. EDX was used to analyze the composition. The thin films band gap changes (1.16–1.28) eV depending on the S/Se ratio in the region where it was discovered. The ratio of sulphur to selenium had an impact on the thin films conductivity and mobility. After thiourea treatment, the CZTSe absorber layer's obtained electrical and optical properties were sufficient for device fabrication [42].

Saha et al. (2021) used a CdS(n)/(Ag_xCu_{1-x})₂ZnSnSe₄ (p) /Cu₂ZnSnSe₄ (p+) structure to improve the efficiency of a CZTSe solar cell. Due to its low manufacturing cost and environmentally friendly ingredients, the direct bandgap of Cu₂ZnSnSe₄ (CZTSe) material is a suitable absorber for thin film photovoltaics. They set the carrier density of each layer so that CZTSe is depleted and the produced minority is efficiently collected. they CZTSe as the back surface absorbent layer to prevent surface recombination and ITO as the back electrode to avoid band bending and increase the open-circuit voltage. They also tune the thicknesses of different layers, resulting in an efficiency of 18.63 % [43].

Karbassi et al. (2021) showed CZTS is an ideal absorbent layer for solar cell manufacturing because of its bandgap of 1.4 to 1.5 eV and low cost of manufacture, making it an effective absorbent layer for solar cells. Cu₂ZnSnS₄ (CZTS) was synthesized using a simple hydrothermal process. According to X-ray diffraction spectroscopy (XRD), the nanoparticles produced by CZTS have a Kesterite structure, the grain size was between 125 and 477 nm. As could be seen in the FESEM image, the annealing process improved the morphology of CZTS thin films, making them more compact [44].

Ghosh et al. (2022) The effects of molybdenum disulfide (MoS₂) as a buffer layer on the various parameters of CZTS-based solar cell devices have been researched in high-efficiency sunlight devices. The CZTS film's band gap was 1.52 eV, and the absorber layer thickness was tuned, ranging from 0.5 μm to 4 μm. Improving upon certain aspects of solar cells' performance: the open circuit voltage is 0.8521 V, and the short circuit current was 25.3 mA /cm², the fill factor was 84.76%, and the efficiency was 18.27% [45].

1.5 Aim of the Work

The aim of this work can be summarized in the following points:

1. Preparation and characteristics study of CZTS and CZTSe powders by Melt quenching and Hydrothermal techniques.
2. Preparation and characteristics study of CZTS and CZTSe thin films using thermal evaporation and spin coating techniques at different annealing temperatures.
3. Fabrication and study I-V properties of CZTS and CZTSe quaternary heterojunction solar cells structure compositions [ITO / CZTS / CdS / ZnO/Al] and [ITO / CZTSe / CdS / ZnO/Al]